Investigation of Temperature Field Evolution in Pangasius Fillets during Freezing

Manuscript received June 17, 2026; revised July 14, 2026

Hoang Thi Nam Huong
Thermal and Refrigeration Technology Department
Ho Chi Minh City University of Technology
Ho Chi Minh City, Viet Nam
htnhuong@hcmut.edu.vn

Do Huu Hoang*
Faculty of Chemical Engineering
Ho Chi Minh City University of Industry and Trade
Ho Chi Minh City, Viet Nam
hoangdh@huit.edu.vn

Abstract— **This study investigates the spatial and temporal evolution of temperature within Pangasius fillets during freezing using a finite element model of two-dimensional nonlinear transient heat conduction with phase change and convective boundary conditions. The model was implemented in ANSYS for a representative fillet cross-section and simulated under an air temperature of −40 °C and air velocity of 10 m/s. Temperature histories at 25 representative nodes were analyzed to characterize local freezing behavior and identify differences between surface and interior regions. The results reveal three characteristic stages: rapid precooling toward 0 °C, a phase-change period dominated by latent heat release, and subsequent sensible cooling after freezing is completed. Surface and corner regions cooled substantially faster than interior locations because of stronger convective heat transfer, while the geometric center exhibited the longest freezing delay. The maximum thermal delay between the corner and center occurred near −3 °C, reaching approximately 800 s, and decreased as the temperature approached the fully frozen state. Below approximately −18 to −20 °C, temperature-time curves exhibited increasingly similar slopes, indicating completion of phase change. These findings demonstrate that temperature-field analysis can support reliable freezing-time prediction and provide a quantitative basis for optimizing operating conditions, energy efficiency, and product quality.**

Keywords— Finite Element Method, Freezing, Pangasius Fillet, Temperature Field Evolution, Transient Heat Conduction

I. INTRODUCTION

Pangasius is one of Vietnam's major seafood export commodities. In recent years, although production has continuously increased, the total export value has not shown a corresponding growth, mainly because some products have failed to satisfy quality requirements and international standards [1]. One of the key factors affecting the quality of processed Pangasius products is the freezing technology employed during processing. A shorter freezing time generally results in better product quality and a longer storage life. However, rapid freezing usually requires a higher refrigeration capacity, leading to increased energy consumption and production costs [1]. Therefore, to simultaneously ensure the quality of frozen Pangasius products and achieve efficient energy utilization, it is necessary to monitor and control the temporal and spatial temperature distribution within the product during the freezing process. To accomplish this objective, a mathematical model describing the freezing process must be developed based on the governing equations of transient heat conduction coupled with third-type (convective) boundary conditions.

The freezing process is highly complex and involves several simultaneous phenomena, including heat transfer, mass transfer, phase change, and variations in the mechanical properties of the product. In particular, near the freezing point, thermophysical properties such as specific heat capacity (c), thermal conductivity (λ), and density (ρ) undergo abrupt changes. As a result, the governing heat conduction equations become strongly nonlinear and difficult to solve. Analytical methods and empirical correlations developed from experimental data have been widely used to estimate freezing times; however, these approaches often yield limited accuracy and do not provide information on the temperature field within the product [2]-[4], [7]-[11],[14]-[19]. Consequently, most recent studies have employed numerical methods to solve the governing equations of the freezing process. Although numerous studies have investigated freezing time and product quality, relatively few have provided a detailed analysis of the evolution of the temperature field during the freezing process, particularly for food products in general and Pangasius fillets in particular. Therefore, investigating the temperature field evolution in Pangasius fillets, as well as in food products more broadly, remains an important and timely research topic. In this study, the finite element method (FEM) is applied to solve the transient heat conduction equations with phase change under third-type (convective) boundary conditions. The developed numerical model is then used to simulate the freezing process of Pangasius fillets and to predict the evolution of the temperature field within the product.

II. MATERIAL AND METHODS

Pangasius fillet samples were obtained from fresh Pangasius harvested in the Mekong Delta region of Vietnam. The dimensions of the fillets were determined based on measurements conducted at a commercial processing plant [13]. The fillets were assumed to have a rectangular slab geometry with the following average dimensions (thickness × width × length, mm): (1) 12 × 70 × 180; (2) 15 × 85 × 200; (3) 18 × 100 × 220; (4) 21 × 115 × 230; and (5) 24 × 125 × 250. Since the thickness and width of the fillets are relatively small compared with their length, heat conduction along the longitudinal direction was neglected. Therefore, the temperature distribution was assumed to vary only in the width direction (denoted as the x-axis) and the thickness direction (denoted as the y-axis), such that: $t = f(x,y,\tau)$. The thermophysical properties of the Pangasius fillets, including specific heat capacity, (c) ($J \cdot kg^{-1} \cdot K^{-1}$), thermal conductivity, λ

 EISSN: 2961-872X ●PISSN: 2961-8924●DOI: 10.56741/IISTR.esl.002436

($W \cdot m^{-1} \cdot K^{-1}$), and density, ρ ($kg \cdot m^{-3}$), were determined according to the correlations reported in [1].

Freezing air conditions: the air temperature in the freezing chamber was maintained at t = - 40 °C, the average velocity of the circulating cold air inside the freezing system was ω = 10 m/s. The convective heat transfer coefficient at the product surface was determined according to the correlation reported in Stoecker [6]:

$$\alpha = 25 \times \omega^{0.6} \left(W \cdot m^{-2} \cdot K^{-1} \right) \quad (1)$$

A. Methodology

Based on the assumptions described above, the temperature within the product was considered to vary only in the two directions of the cross-section. Therefore, it was sufficient to determine the temperature distribution over a representative cross-section of the Pangasius fillet. To solve the transient heat conduction equation using the finite element method (FEM), the cross-section was discretized into a computational mesh. The mesh was generated using an orthogonal grid with uniform spacings (Δx) and (Δy), where (Δx = Δy). Owing to the geometric symmetry of the cross-section, the temperature field was evaluated only within one-quarter of the domain, corresponding to nodes 1–25 (Fig. 2). The computational domain was discretized using four-node first-order rectangular elements (Quad 4-node Plane 55 elements). A structured mesh with uniform element size was employed throughout the domain, as illustrated in Fig. 1.

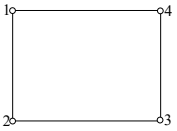


Fig. 1. Four-node rectangular element

To evaluate the evolution of the temperature field during the freezing process, several representative nodes were selected for detailed analysis (Fig. 2). Since the finite element model consisted of a mesh containing (5 × 55) elements, the computed temperature field data were highly dense, making a point-by-point analysis impractical. Therefore, representative nodal locations were chosen to characterize the temperature distribution and its temporal evolution within the product. The sample selected for the analysis had dimensions of 15 mm × 85 mm (thickness × width). Due to the symmetry of the computational domain, only one-quarter of the cross-section was considered in the numerical calculations.

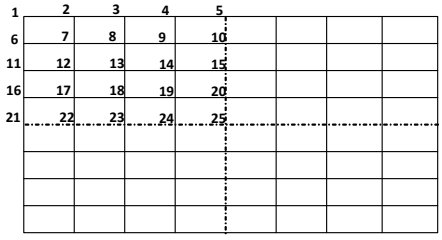


Fig. 2. Representative nodal locations for temperature field analysis in the cross-section of the Pangasius fillet.

B. Mathematical model development

The arrangement of Pangasius fillet samples on a straight Individual Quick Freezing (IQF) conveyor is illustrated in Fig. 3.

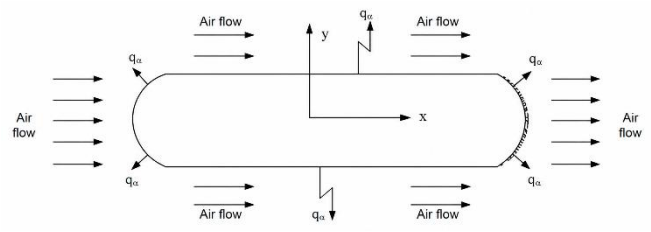


Fig. 3. Product arrangement.

Based on the assumptions presented in Section 2.1, the freezing process can be formulated as a two-dimensional nonlinear transient heat conduction problem with phase change, governed by the corresponding initial condition and third-type (convective) boundary conditions as follows:

Heat Conduction Differential Equation:

$$\lambda(T)\left(\frac{\partial^2 T}{\partial x^2}+\frac{\partial^2 T}{\partial y^2}\right)+q_V=\rho(T)C_P(T)\frac{\partial T}{\partial \tau} \quad (2)$$

Initial Condition:

$$\tau = 0 \Rightarrow T = T(x,y,0) = 12^{o}C \quad (3)$$

Symmetric Robin Boundary Condition

$$\begin{cases} \left(\dfrac{\partial T}{\partial x}\right)_{x=0} = \left(\dfrac{\partial T}{\partial y}\right)_{y=0} = 0 \\ \pm\left(\dfrac{\partial T}{\partial x}\right)_{x=\pm\delta_x} = \pm\dfrac{\alpha}{\lambda(T)}\left(T-T_f\right)_{x=\pm\delta_x} \\ \pm\left(\dfrac{\partial T}{\partial y}\right)_{y=\pm\delta_y} = \pm\dfrac{\alpha}{\lambda(T)}\left(T-T_f\right)_{y=\pm\delta_y} \end{cases} \quad (4)$$

The nonlinear transient freezing problem was solved using the finite element method. Employing the Galerkin formulation [12], the governing heat conduction equation given in Eq. (5) was discretized and expressed in the following finite element matrix form:

$$[C]\left\{\frac{\partial t}{\partial \tau}\right\}+[K]\{t\}=\{f\} \quad (5)$$

where:

$[C]=\left[\int_V\left(\rho.c[N]^T[N]\right)dV\right]$ is the heat capacity matrix;

$[K]=\left[\int_V\left(\lambda[B]^T[B]\right)dV+\int_S\left(\alpha[N]^T[N]\right)dV\right]$ is the thermal conductivity matrix;

$\{f\}=\int_S[N]^T q_V dS-\int_S[N]^T q dS+\int_S\alpha[N]^T T_K dS$ is the load vector.

The general form of the solution to Eq. (5) is given by

$$\{[C]+\theta.\Delta\tau[K]\}\{T\}^{p+1}=\{[C]-(1-\theta)\Delta\tau[K]\}\{T\}^{p}+\Delta\tau\{\theta\{f\}^{p+1}+(1-\theta)\{f\}^{p}\} \quad (6)$$

Where (θ) is a weighting parameter satisfying [0 ≤θ ≤ 1]. Accordingly, the solution of Eq. (6) can be rewritten as follows:

For (θ = 0), Eq. (6) is solved using the explicit time-integration scheme:

$$T^{p+1}=[C]^{-1}*\left[\left([C]-[K]\Delta\tau\right)\{T^p\}+\{f^p\}\Delta\tau\right] \quad (7)$$

For (θ = 1), Eq. (4) is solved using the implicit time-integration scheme:

$$T^{p+1}=\left[[C]-[K]\Delta\tau\right]^{-1}*\left[[C]T^p+\{f^{p+1}\}\Delta\tau\right] \quad (8)$$

For ($\theta = 1/2$), the Crank–Nicolson (semi-implicit) scheme is obtained:

$$\{[C]+0{,}5\Delta\tau[K]\}\{T\}^{p+1} = \{[C]-0{,}5\Delta\tau[K]\}\{T\}^{p}+0{,}5\Delta\tau\left(\{f\}^{p+1}+\{f\}^{p}\right) \quad (9)$$

C. *Simulation of the freezing process*

The numerical simulations were performed using ANSYS software. Equation (4) was solved using the fully explicit scheme ($\theta = 0$). In principle, the solution remains convergent for arbitrary values of the time step ($\Delta\tau$). However, larger time-step sizes generally lead to reduced numerical accuracy. Therefore, for the fully explicit formulation represented by Eq. (7), a time step of ($\Delta\tau$ =5 s) was adopted. The freezing process was simulated under operating conditions corresponding to an air velocity of (ω = 10 m.s^{-1}) and an air temperature of (t = - 40 °C). The simulated temperature distributions across the cross-section of the fillet are presented in Fig. 4.

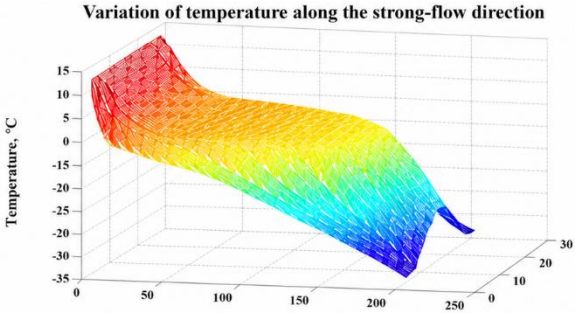


Fig. 4. Temperature distribution in the fillet cross-section

D. *Evaluation of the Reliability of the Problem Solution*

During the freezing process, the deviation between theoretically and experimentally computed temperatures is not equal [20]-[25]. In the precooling stage, the temperature difference does not exceed 1.0 K; in the phase change stage, the temperature difference does not exceed 1.5 K; in the subcooling stage, the temperature difference does not exceed 4K. However, considering the complexity of the process, especially the sudden variation of thermophysical properties at the freezing point, this difference is acceptable and this theoretical model can be applied with high reliability to study the freezing process of many kinds of food.

III. Results and Discussion

A. *Temperature evolution of the 25 nodal points on the cross-section*

Based on the simulation results presented in Fig. 5. Temperature histories at the 25 selected nodes the following observations can be made.

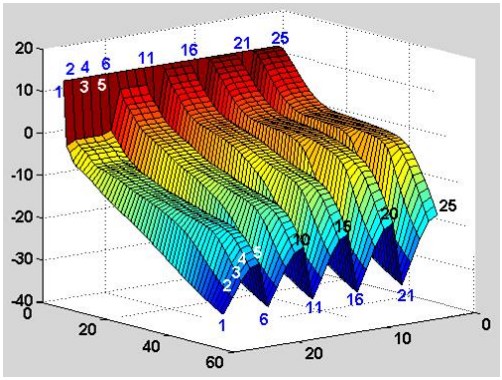


Fig. 5. Temperature histories at the 25 selected nodes.

Based on the simulation results presented in Fig. 5, the temperature variations within the horizontal layers exhibit similar characteristics. Layer 1 consists of nodes 1, 2, 3, 4, and 5; Layer 2 consists of nodes 6, 7, 8, 9, and 10; Layer 3 consists of nodes 11, 12, 13, 14, and 15; Layer 4 consists of nodes 16, 17, 18, 19, and 20; and Layer 5 consists of nodes 21, 22, 23, 24, and 25. The temperature–time curves corresponding to these layers display similar profiles and follow the same overall trend. This behavior can be explained by the following observations:

- The temperature histories at nodes 1, 6, 11, 16, and 21 exhibit similar profiles.
- Likewise, the temperature histories at nodes 2, 7, 12, 17, and 22 show similar behavior
- Similar trends are also observed for the groups of nodes 3, 8, 13, 18, and 23; nodes 4, 9, 14, 19, and 24; and nodes 5, 10, 15, 20, and 25.

Consequently, the temperature evolution patterns of the different horizontal layers are essentially identical.

- The surface nodes (1, 6, 11, 16, and 21) exhibit the highest cooling rates and attain the lowest temperatures during the freezing process. This can be attributed to their location on the exposed surface directly facing the cold-air flow, where convective heat transfer is most intense. Among these nodes, node 1 reaches the lowest temperature, approximately (-33.57 C), at (52 =1003,75s);
- The interior nodes cool more slowly than the surface nodes. The slowest cooling rates are observed at nodes 5, 10, 15, 20, and 25, which are located furthest from the exposed surface. Among them, node 25 maintains the highest temperature during the freezing process, reaching only (-18,22 °C) at the same time instant;

These observations are consistent with the physical heat-transfer mechanisms occurring during freezing. The outer layers, which are directly exposed to the low-temperature air stream, experience rapid heat removal and therefore cool quickly. The adjacent subsurface layers also cool relatively rapidly due to the large temperature gradients between the surface and the interior. In contrast, the inner regions of the fillet are located farther from the cooling surface, resulting in lower heat-conduction rates and consequently a slower temperature decrease.

 EISSN: 2961-872X ●PISSN: 2961-8924●DOI: 10.56741/IISTR.esl.002436

B. Temperature evolution at the upper surface of the product

The upper surface of the product is represented by nodes 1, 2, 3, 4, and 5. The temperature histories at these representative locations during the freezing process are presented in Fig. 6.

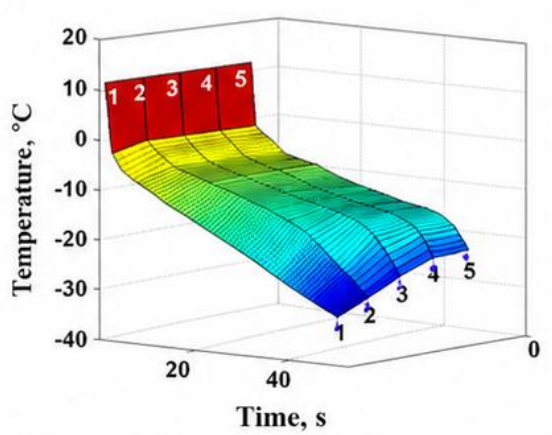


Fig. 6. Temperature histories at representative nodes on the upper surface of the product.

Fig. 78 illustrates the temperature variation and distribution at nodes 1–5.

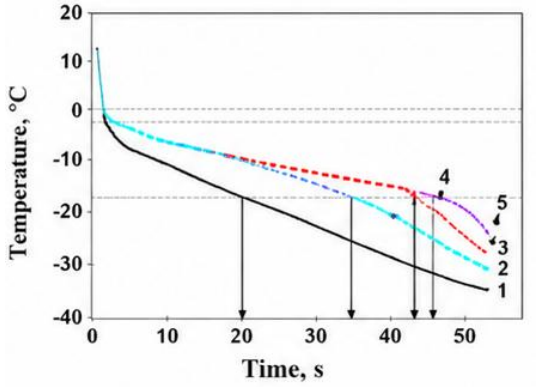


Fig 7. Temperature variation and distribution at nodes 1–5.

Fig. 8 illustrates the temperature distribution along the upper surface during the freezing process.

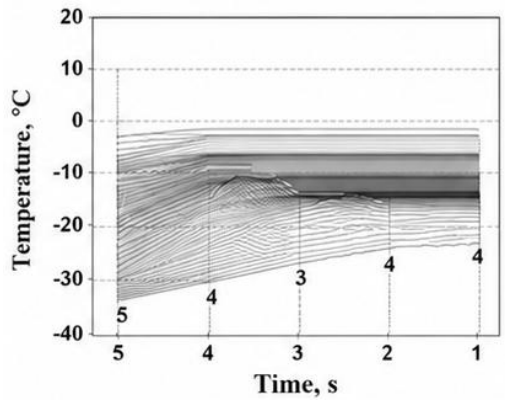


Fig. 8. The temperature distribution along the upper surface during the freezing process.

Observations:

Immediately after exposure to the cold-air stream, the temperature at the upper surface decreases rapidly and falls below (0 °C); Once the temperatures at the monitored nodes reach approximately (-3 °C), the cooling rate decreases, and the temperature–time curves become progressively less steep;

Node 1 consistently exhibits a lower temperature than the other surface nodes. In addition, its cooling rate remains nearly uniform throughout the freezing process. This behavior can be attributed to the fact that node 1 is located at a corner element, where heat is removed simultaneously from two exposed surfaces. Consequently, the local heat-transfer rate is higher, resulting in a faster and more uniform temperature decrease, as well as a lower final temperature compared with the other nodes.

Nodes 2, 3, 4, and 5 exhibit lower cooling rates than node 1 during most of the freezing process. However, near the end of the process, when their temperatures decrease to approximately (– 18 °C), the cooling rate increases, as indicated by the steeper temperature–time curves. This behavior can be explained by the release of latent heat during water crystallization within the product. During the phase-change period, the latent heat of freezing slows the temperature decrease considerably. When the temperature approaches approximately (– 18 °C), the water contained in the product is assumed to be completely frozen. Below this temperature, the slopes of the temperature curves become nearly constant, indicating that no further phase change occurs and that heat transfer is governed primarily by sensible heat conduction.

A significant difference is observed in the time required to achieve complete freezing at node 1 compared with nodes 2, 3, 4, and 5. Relative to node 1, complete freezing occurs approximately 300 s later at node 2, 440 s later at node 3, and 500 s later at nodes 4 and 5. These results demonstrate the strong influence of spatial location on the freezing behavior and temperature evolution within the product.

C. Temperature evolution at the front surface of the product (Nodes 1, 6, 11, 16, and 21)

The temperature histories at the front surface of the product, represented by nodes 1, 6, 11, 16, 21, are presented in Fig. 9.

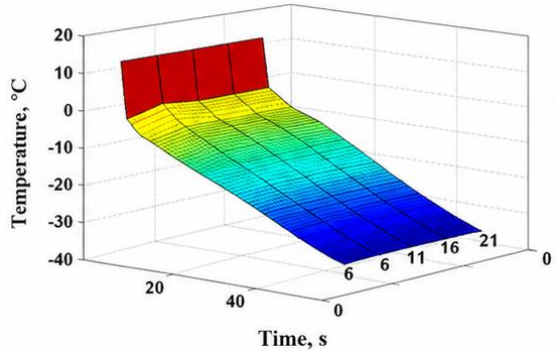


Fig. 9. Temperature histories at representative nodes on the front surface of the product.

The corresponding temperature evolution and temperature distribution across the front surface during the freezing process are illustrated in Fig. 10 and Fig.11, respectively.

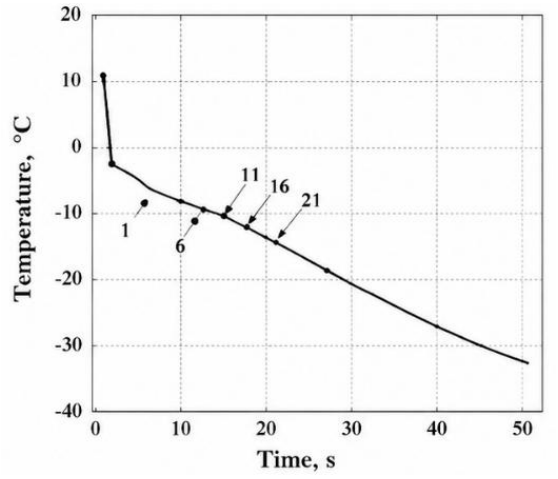


Fig. 10. Temperature evolution at nodes 1, 6, 11, 16, and 21.

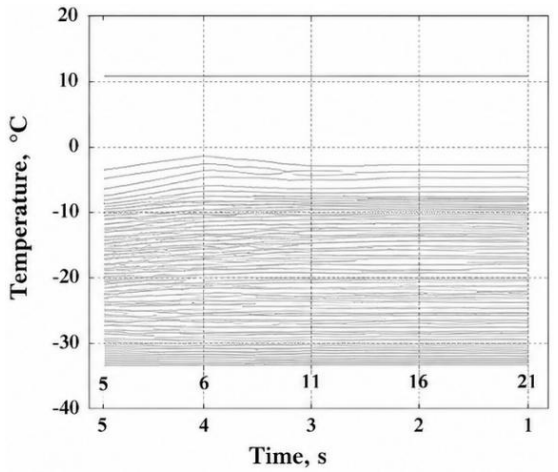


Fig. 11. Temperature distribution along the front surface during the freezing process.

Observations:

The temperature evolution on the front surface can be represented by an almost planar inclined surface, indicating that the temperature decreases relatively uniformly across this surface during the freezing process.

The temperature–time curves clearly show noticeable temperature differences among the selected nodes when the temperature is above approximately (-20 ºC). However, below (-20 ºC), the temperature differences become negligible. The temperature histories nearly coincide and exhibit similar slopes, while the corresponding temperature-distribution curves become almost horizontal.

These results suggest that complete freezing at the investigated nodes occurs at approximately (-20 ºC). Below this temperature, the thermal behavior is essentially identical at all nodes, indicating that the phase-change process has been completed and that the subsequent temperature decrease is governed primarily by heat conduction.

D. Temperature evolution along the vertical line through Nodes 5, 10, 15, 20, and 25

The temperature histories of the product, represented by nodes 1, 6, 11, 16, 21, are presented in Fig. 12.

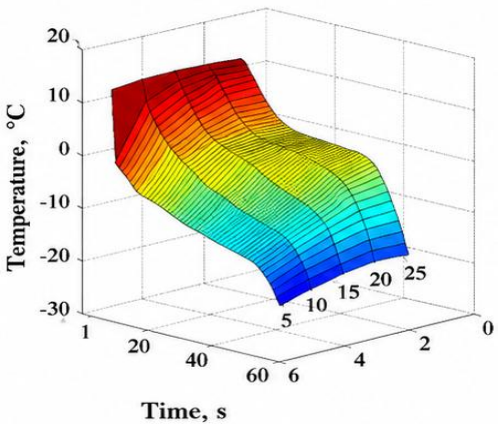


Fig. 12. Temperature histories at nodes 5, 10, 15, 20, and 25.

The temperature field exhibits a pronounced spatial gradient from the surface toward the center of the product, resulting in substantially different temperature histories at the investigated nodes This behavior is expected because the nodes are located at different depths, extending from the product surface toward its geometric center.

The spatial and temporal temperature differences among the nodes are clearly illustrated in Figs. 13 and 14.

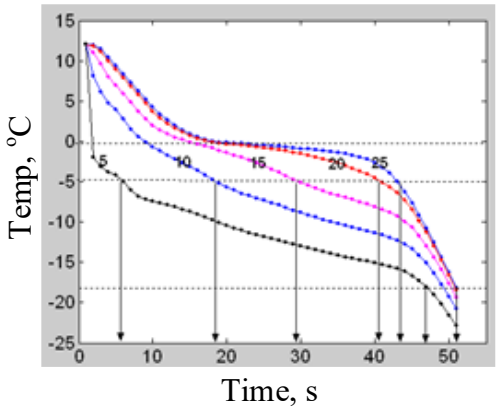


Fig. 13. Temperature evolution along the selected vertical line.

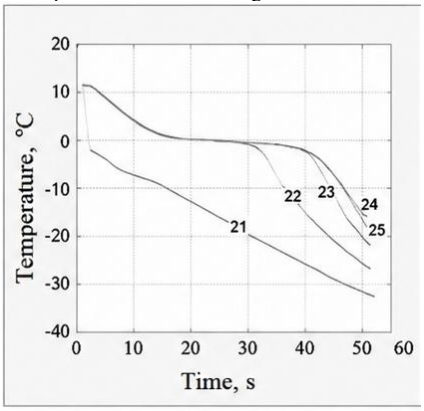


Fig. 14. Temperature distribution along the selected vertical line during the freezing process.

Significant differences are observed in the time required for the nodes to reach the same temperature. The largest discrepancy occurs at approximately (-5 ºC). As shown in Fig. 12, node 5 reaches (-5 ºC) at time step 6 (120s); node 10 reaches the same temperature at time step 19, corresponding to a delay of 13 time steps (260s); node 15 at time step 29, corresponding to a delay of 23 time steps (460s); node 20 at time step 40, corresponding to a delay of 34 time steps (680s);

 EISSN: 2961-872X ●PISSN: 2961-8924●DOI: 10.56741/IISTR.esl.002436

and node 25 at time step 43, corresponding to a delay of 37 time steps (740s).

The time difference required for the nodes to reach the same temperature decreases as the temperature becomes lower. At approximately (-18 ºC), the maximum time difference between nodes 5 and 25 is only five time steps, corresponding to approximately (100s).

Below (-18 ºC), the temperature–time curves exhibit nearly identical slopes, while the temperature-distribution profiles approach a slightly inclined straight line. This behavior indicates that all investigated locations have reached a fully frozen state. At this stage, the latent heat associated with the phase-change process has been completely released, and heat transfer is governed solely by sensible cooling, resulting in a nearly uniform rate of temperature decrease throughout the product.

E. Temperature evolution along the horizontal line through Nodes 21, 22, 23, 24, and 25

The temperature histories at nodes 21, 22, 23, 24, and 25, are presented in Fig. 15.

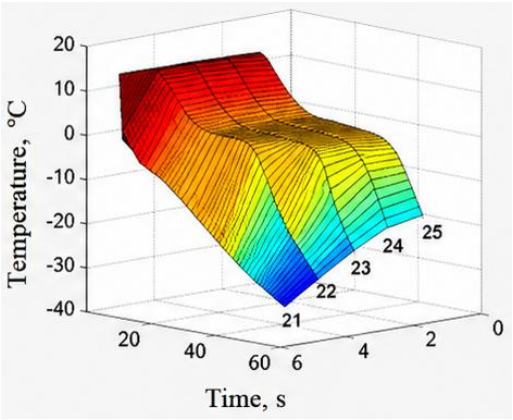


Fig. 15. Temperature histories at nodes 21, 22, 23, 24, and 25.

The corresponding temperature evolution and temperature distribution at nodes 21, 22, 23, 24, and 25 during the freezing process are illustrated in Fig. 16 and Fig. 17, respectively.

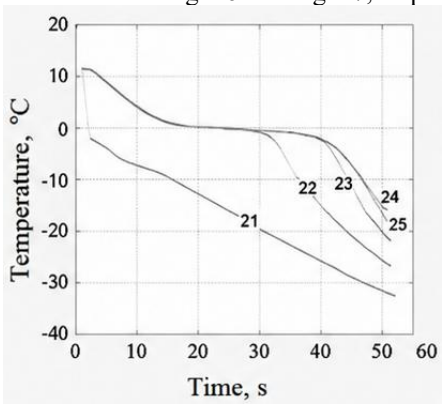


Fig. 16. Temperature evolution along the selected horizontal line.

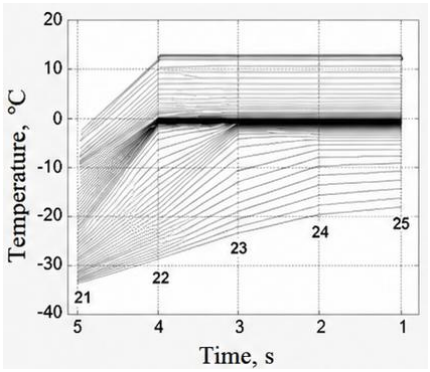


Fig. 17. Temperature distribution along the selected horizontal line during the freezing process.

Observations:

The temperature evolution along the horizontal line passing through nodes 21, 22, 23, 24, and 25 forms an inclined and non-uniform surface, indicating significant temperature differences among these locations. This behavior can be attributed to the fact that the nodes are situated at different positions along the horizontal direction, extending from the exposed surface toward the interior of the product. Consequently, the heat-transfer conditions and cooling rates vary from one node to another;

The temperature–time curves show that the profiles corresponding to nodes 22, 23, 24, and 25 nearly overlap and remain almost horizontal between time steps 18 and 25, indicating that their temperatures remain approximately constant at (0 ºC) during this period. This temperature plateau is characteristic of the phase-change process, during which the latent heat released by water crystallization counterbalances the heat removed from the product, resulting in little or no temperature decrease despite continued cooling.

F. Differences in freezing time and temperature evolution characteristics at representative locations

To investigate the differences in freezing time among various locations within the product, nodes exhibiting the largest temperature differences were selected for analysis. These include node 1, located at the corner of the cross-section on the external surface of the product, and node 25, located at the geometric center of the product. These two nodes are separated by the greatest distance within the analyzed cross-section and therefore represent the most extreme thermal conditions. In addition, node 13, situated approximately midway between nodes 1 and 25, was selected as an intermediate location to evaluate the temperature evolution characteristics within the product. The differences in freezing time and the corresponding temperature histories at these representative nodes are presented in Fig. 18.

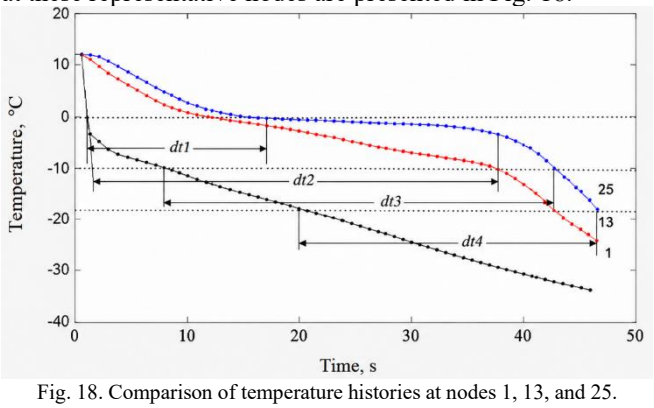


Fig. 18. Comparison of temperature histories at nodes 1, 13, and 25.

Observations:

The time lag required for node 25 to reach the same temperature as node 1 is denoted by dT. Figure 9 illustrates the corresponding delays at several characteristic temperatures: dT_1 for (0 ºC), dT_2 for (- 3 ºC), dT_3 for (- 10 ºC), and dT_4 for (- 18 ºC). Specifically:

- Node 1 reaches (0 ºC) shortly before time step 2 (8s), whereas node 25 reaches the same temperature at time step 20 (400s). Therefore, the corresponding time lag is (dT_1 = 392s);
- At (- 3 ºC), node 1 reaches this temperature at time step 1 (20s), while node 25 reaches it at time step 41 (820s), resulting in a time lag of (dT_2 = 800s);
- At (-10 ºC), node 1 reaches the target temperature at time step 10 (200s), whereas node 25 reaches it at time step 47 (940s). The corresponding delay is (dT_3 = 740s);
- At (-18 ºC), node 1 reaches the target temperature at time step 23 (460s), while node 25 does not reach this temperature until time step 52 (1040s). Consequently, the time lag is (dT_4 = 580s);
- It can be observed that the largest time lag occurs at (-3 ºC) (dT_2), followed by the time lag at (-10 ºC) (dT_3), and then at (-18 ºC) (dT_4);
- In other words, the most significant thermal delay occurs within the temperature range from approximately (-3 ºC) to (-10 ºC).

These findings provide useful insights for selecting appropriate freezing conditions and operating temperatures to reduce the overall freezing time and improve process efficiency. The temperature evolution characteristics at the selected nodes can be described as follows.

Node 1: The temperature–time curve exhibits a very steep initial decline, indicating rapid heat removal caused by intense convective heat transfer at the exposed surface. Subsequently, the slope decreases as latent heat is released during the freezing process. After approximately time step 4, the negative slope becomes relatively uniform, suggesting that the heat gained from adjacent internal regions and the heat lost to the surrounding cold air remain approximately balanced and stable throughout the remainder of the freezing process.

Nodes 13 and 25: The temperature–time curves also show a relatively steep initial decrease. However, between approximately time steps 15 and 40, their negative slopes become smaller than that of node 1. This behavior is attributed to the release of latent heat associated with water crystallization, which slows the temperature decrease. After time step 40, the negative slopes increase again, indicating a more rapid temperature reduction. This phenomenon can be explained by the increase in effective thermal conductivity after the phase-transition region, which enhances heat conduction within the product and accelerates the cooling process.

The temperature–time curve corresponding to node 25 remains above that of node 13 throughout the freezing process. This behavior is attributed to the location of node 25 deeper within the product, where heat removal is less effective than at node 13. Consequently, the temperature at node 25 decreases more slowly and remains higher than that at node 13 at any given time.

The aforementioned characteristics are also evident from the temperature evolution observed at nodes located in different layers of the product, as illustrated in Fig. 7(b), which presents the temperature variation along the line passing through nodes 5, 10, 15, 20, and 25, and Fig. 8(b), which shows the temperature variation along the line passing through nodes 21, 22, 23, 24, and 25. In both cases, the temperature histories reveal the influence of spatial position on the cooling rate and freezing behavior within the product.

IV. Conclusions

The numerical results obtained in this study are consistent with the physical phenomena observed during the freezing process. When Pangasius fillets are exposed to a cold-air environment, the temperatures at different locations within the product evolve through three distinct stages:

- **Stage 1:** A rapid temperature decrease from the initial positive temperature to approximately (0 °C). This stage is characterized by a steep temperature gradient due to intense convective heat transfer at the product surface;
- **Stage 2:** The phase-change stage, during which the temperature–time curves become less steep and approach a plateau. The release of latent heat associated with water crystallization slows the temperature decrease considerably;
- **Stage 3:** A subsequent period of relatively rapid cooling following the completion of phase change. During this stage, the effective thermal conductivity of the product increases, enhancing heat transfer within the fillet. As a result, the temperatures at all locations continue to decrease and gradually approach the ambient air temperature.

The extent to which these three stages are manifested depends strongly on the spatial location within the product. The thermal behavior at each node is influenced by its distance from the cooling surface and the associated heat-transfer conditions.

At the front surface, and particularly at the corner regions of the product, heat removal is most intense, resulting in a rapid temperature decrease and a very short freezing period. Consequently, the phase-change stage is scarcely distinguishable at these locations. In contrast, all interior nodes clearly exhibit the three characteristic stages described above. Moreover, the duration of the phase-change stage increases with increasing distance from the surface. This stage is most pronounced at the geometric center of the product, where the freezing process takes the longest time to complete.

Based on the characteristic three-stage temperature evolution observed at each location within the product, it is possible to predict the temperature and time corresponding to complete freezing. Such information can provide a useful basis for determining an appropriate freezing duration, thereby ensuring product quality while improving the efficiency of the freezing process.

References

[1] H. H. Đỗ, *Numerical Simulation and Determination of Optimal Freezing Conditions for Vietnamese Pangasius*, Ph.D. dissertation, Hanoi University of Science and Technology, Hanoi, Vietnam, 2014.

 EISSN: 2961-872X ●PISSN: 2961-8924●DOI: 10.56741/IISTR.esl.002436

[2] A. C. Cleland and R. L. Earle, "A comparison of analytical and numerical methods of predicting the freezing times of foods," *J. Food Sci.*, vol. 42, pp. 1390–1395, 1977.

[3] A. C. Cleland and R. L. Earle, "Predicting freezing times of food in rectangular packages," *J. Food Sci.*, vol. 44, pp. 964–970, 1979.

[4] A. K. Fleming, "Immersion freezing small meat products," in *Proc. 12th Int. Congr. Refrigeration*, Madrid, Spain, vol. 2, 1967, pp. 683–694.

[5] C. Lacroix and F. Castaigne, "Simple method for freezing time calculations for infinite flat slabs, infinite cylinders and spheres," *Can. Inst. Food Sci. Technol. J.*, vol. 20, pp. 251–259, 1987.

[6] W. F. Stoecker, *Industrial Refrigeration Handbook*. New York, NY, USA: McGraw-Hill, 2004, ch. 17, pp. 567–589.

[7] J. Succar and K. Hayakawa, "Parametric analysis for predicting freezing time of infinitely slab-shaped food," *J. Food Sci.*, vol. 49, pp. 468–477, 1984.

[8] Q. T. Pham, "An approximate analytical method for predicting freezing times for rectangular blocks of foodstuffs," *Int. J. Refrig.*, vol. 8, pp. 3–47, 1985.

[9] Q. T. Pham, "Extension to Plank's equation for predicting freezing times of foodstuffs of simple shapes," *Int. J. Refrig.*, vol. 7, pp. 377–383, 1984.

[10] R. Plank, "Beiträge zur Berechnung und Bewertung der Gefriergeschwindigkeit von Lebensmitteln," *Zeitschrift für die gesamte Kälte-Industrie*, Beih. Reihe 3, no. 10, pp. 1–16, 1941.

[11] R. H. Mascheroni and A. Calvelo, "A simplified model for freezing time calculations in foods," *J. Food Sci.*, vol. 47, pp. 1201–1207, 1982.

[12] R. W. Lewis, P. Nithiarasu, and K. N. Seetharamu, *Fundamentals of the Finite Element Method for Heat and Fluid Flow*. Chichester, U.K.: John Wiley & Sons, 2004, pp. 154–170.

[13] A. Avadí, I. Vázquez-Rowe, A. Symeonidis, and E. Moreno-Ruiz, "First series of seafood datasets in ecoinvent: Setting the pace for future development," *Int. J. Life Cycle Assess.*, vol. 25, no. 7, pp. 1333–1342, 2020, doi: 10.1007/s11367-019-01659-x.

[14] Z. Huan, S. He, and Y. Ma, "Numerical simulation and analysis for quick-frozen food processing," *J. Food Eng.*, vol. 60, no. 3, pp. 267–273, 2023.

[15] F.-L. Tan and S.-C. Fok, "Freezing of tilapia fillets in an air blast freezer," *Int. J. Food Sci. Technol.*, vol. 44, no. 8, pp. 1619–1625, 2009.

[16] J. Dima, M. Santos, P. Baron, A. Califano, and N. Zaritzky, "Experimental study and numerical modeling of the freezing process of marine products," *Food Bioprod. Process.*, vol. 92, no. 1, pp. 54–66, 2014.

[17] H. T. T. Dang, M. Gudjónsdóttir, T. Tómasson, M. V. Nguyen, M. G. Karlsdóttir, and S. Arason, "Influence of processing additives, packaging and storage conditions on the physicochemical stability of frozen Tra catfish (*Pangasius hypophthalmus*) fillets," *J. Food Eng.*, vol. 238, pp. 148–155, 2018.

[18] P. Ye, K. Luo, A. Feng, D. Zhao, D. Wang, X. Lin, and Z. Liu, "Magnetic field improves the quality of frozen tilapia fillets by decreasing the ice crystals during freezing process," *Int. J. Food Sci. Technol.*, vol. 59, no. 12, pp. 8961–8971, 2024.

[19] A. Biglia, L. Comba, E. Fabrizio, P. Gay, and D. R. Aimonino, "Case studies in food freezing at very low temperature," *Energy Procedia*, vol. 101, pp. 305–312, 2016, doi: 10.1016/j.egypro.2016.11.039.

[20] H. H. Do, P. Q. Dang, and D. V. Nguyen, "Determining the time to freeze catfish by applying the finite element analysis," in *Proc. 3rd Int. Conf. Sustainable Energy*, 2013.

[21] H. H. Do and T. N. H. Hoang, "Evaluation of factors influencing the freezing time of the Pangasius fillets," in *Lecture Notes in Mechanical Engineering*. Springer, 2022, pp. 12–28.

[22] V. V. Sim, H. H. Do, and T. N. H. Hoang, "Simulation of beef freezing process and evaluation of influencing factors," *Appl. Mech. Mater.*, vol. 914, pp. 83–94, 2023.

[23] D. K. Hoang, S. J. Lovatt, J. R. Olatunji, and J. K. Carson, "Experimental measurement and numerical modelling of cooling rates of bulk-packed chicken drumsticks during forced-air freezing," *Int. J. Refrig.*, vol. 114, pp. 165–174, 2020.

[24] D. K. Hoang, S. J. Lovatt, J. R. Olatunji, and J. K. Carson, "Validated numerical model of heat transfer in the forced air freezing of bulk packed whole chickens," *Int. J. Refrig.*, vol. 118, pp. 93–103, 2020.

[25] V. V. Sim and H. H. Hoàng, "Mô phỏng cấp đông thịt heo nửa con bằng Ansys," *Tạp chí Năng lượng Nhiệt*, no. 156, pp. 10–16, 2021.